

Cite this: *J. Mater. Chem. C*, 2018, **6**, 726Received 4th December 2017,
Accepted 22nd December 2017

DOI: 10.1039/c7tc05556k

rsc.li/materials-c

Circularly polarized electroluminescence by controlling the emission zone in a twisted mesogenic conjugate polymer†

Jin-Hyung Jung,‡ Dong-Myung Lee,‡ Jae-Hoon Kim and Chang-Jae Yu *

This study describes the degree of circularly polarized electroluminescence defined by a dissymmetry g factor, depending on the emission zone in a twisted mesogenic conjugate polymer. Using a matrix analysis and a ratio of non-polarized emission, the emission zone and the corresponding g factor were quantitatively analysed without additional layers.

Introduction

The emission of polarized light from conjugated polymers with the mesogenic phase is widely studied in both scientific interest and technical applications.^{1–4} In particular, the circularly polarized (CP) emission has attracted much attention in applications such as displays, optical information, and sensing, since the CP emission leads to enhancement in device performance.^{5–8} The degree of CP emission is defined by the dissymmetry g factor $g = 2(I_L - I_R)/(I_L + I_R)$, where I_L and I_R represent the intensities of left-handed CP (LHCP) light and right-handed CP (RHCP) light, respectively. In organic light-emitting diodes (OLEDs), the high $|g|$ value enhances the luminance efficiency in an anti-reflection environment.^{5,6} Recently, a very high $|g|$ value was reported in the doped lanthanide complex. Here, the role of the position of the electron–hole recombination (emission) zone was discussed to achieve high g factor considering the attenuation of emitted light.⁹ It was theoretically expected that the g factor in an induced twist structure of the mesogenic conjugate polymer was varied by the emission zone using a Müller matrix analysis for a twisted birefringent medium.⁶

Probing and controlling the emission zone is crucial to improve the stability of the OLED as well as to understand the degradation mechanism.^{10,11} A well-known approach towards probing the emission zone is to add a thin electroluminescence (EL) layer with different wavelengths at various positions within

the emitting layer (EML).^{11–15} However, such an approach might be questionable since the additional layers give rise to undesirable motion of charge carriers within the EML. Recently, the modelling methodologies using photoluminescence (PL) and EL degradation¹⁰ or using spectrum analysis for two different emitting materials¹⁶ were reported to determine the emission zone. Although these approaches quantitatively described the emission zone, these methods have limitations in the application of various emitting materials.

In this work, we investigate the effect of position of the emission zone on the g factor in the twisted mesogenic conjugate polymer to obtain a high g factor for enhancing the OLED luminance. The relationship between the emission zone and the g factor was directly calculated using the Müller matrix analysis for the continuously twisted configuration of the mesogenic conjugate polymer. The position of the emission zone was controlled by the thickness of a hole blocking layer (HBL), which also acts as an electron injecting hurdle (EIH). We quantitatively determined the emission zone by comparing the measured g factor and the expected g factor associated with the emission zone. It is found that the g factor increases when the emission zone moves toward the cathode but rather decreases when the emission zone enters the HBL due to non-polarized emissions at the HBL for the thicker HBLs. Also, the penetration of the emission zone toward the HBL was analysed with a ratio of non-polarized intensity to polarized intensity and a peak ratio of the emissions at the EML and the HBL.

Experimental

Materials

For the emitting layer, the conjugate polymer, poly(9,9-di-*n*-octylfluorenyl-2,7-diyl)-*alt*-(benzo [2,1,3] thia-diazol-4,8-diyl) (F8BT) and the left-handed chiral dopant, S5011 were commercially acquired from Solaris Chem and Merck, respectively. The F8BT shows a nematic LC phase over 125 °C and the S5011 with a high helical twisting power (HTP) over 100 μm^{-1} for small-molecule LCs¹⁷ exhibits a HTP of about 10 μm^{-1} for the F8BT.⁶ The hole

Department of Electronic Engineering, Hanyang University, Seoul 04763, Republic of Korea. E-mail: cgyu@hanyang.ac.kr

† Electronic supplementary information (ESI) available. See DOI: 10.1039/c7tc05556k

‡ These authors contributed equally.

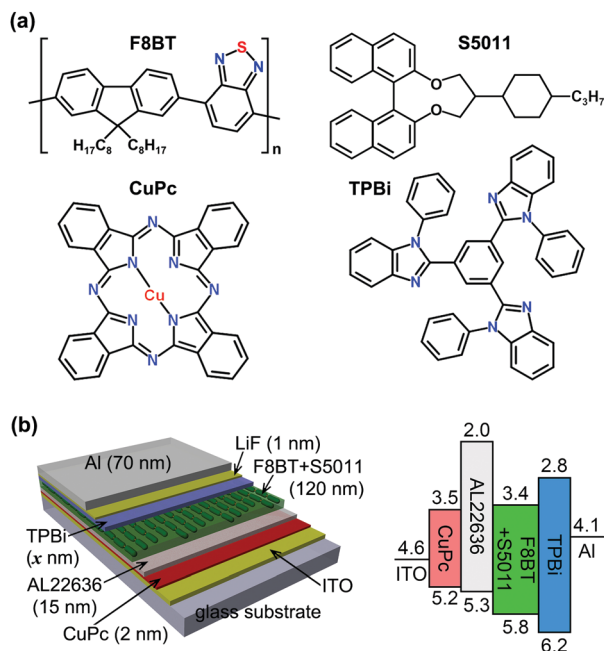


Fig. 1 (a) Chemical structures of the materials, and (b) device configurations and energy level diagrams of the OLEDs in this work.

blocking material, 2,2',2''-(1,3,5-benzotriyl)tris(1-phenyl-1H-benzimidazole) (TPBi) and the hole injection material, copper phthalocyanine (CuPc) were commercially acquired from LUMTEC. For aligning the F8BT, the rubbed alignment layer AL22636, which served as the hole transport layer and the electron blocking layer, was commercially acquired from Japan Synthetic Rubber. All materials were used directly without further purification. The chemical structures of the used materials are shown in Fig. 1a.

Device fabrication

The OLEDs with various thicknesses of the TPBi on the S5011-doped F8BT layer were fabricated in this work. The device structures and energy levels are illustrated in Fig. 1b. Prepatterned indium-tin-oxide (ITO) substrates (a sheet resistance $\approx 20 \Omega \square^{-1}$) were cleaned by ultrasonication in deionized water and mucasol (alkali detergent) for 60 min. The CuPc, served as a hole injection layer, with a thickness of 2 nm was deposited by thermal evaporation under a vacuum of 6×10^{-6} Torr on the ITO surface. To align the EML, the AL22636 was spin-coated (at 1000 rpm for 10 s and 3000 rpm for 20 s) on the CuPc and unidirectionally rubbed by a rubbing machine after imidizing the alignment layer *via* baking at 210 °C for 60 min. The rubbing machine consists of a 6.5 cm-diameter roller covered with a cotton cloth. The rotational speed of the roller and the translational speed of the substrate stage were fixed at 500 rpm and 6 mm s⁻¹, respectively.¹⁸ The dissolved F8BT mixture blended with 7 wt% S5011 in toluene (25.11 mg mL⁻¹) was spin-coated (at 1000 rpm for 10 s and 3000 rpm for 20 s) on the rubbed AL22636 and baked at 150 °C for 10 min (the thickness of the F8BT is 120 nm). The total twisted angle of the F8BT layer was evaluated to be 86° (see the ESI†). TPBi with various thicknesses (0, 10, 20, 30, 40, and 50 nm), LiF (1 nm), and Al (70 nm) were

sequentially deposited by thermal evaporation. All samples were encapsulated by glass and UV curable resin (NOA 65 form Norland Products) under a nitrogen atmosphere to avoid exposure to oxygen and humidity.

Device characterization

The linearly polarized photoluminescence (LPPL) and the CP electroluminescence (CPEL) of the OLEDs were measured using a spectroradiometer (TOPCON, SR-UL 1R) under a rotary stage. The birefringence of the F8BT was measured using the photoelastic modulator (PEM) (Hinds, PEM-100) and the lock-in amplifier (Stanford Research System, SR830) based on the PEM method (see the ESI†). The LPPL was measured using the intensity ratio of the parallel component to the aligned direction of the F8BT to the perpendicular one. The CPEL was observed under a circular polarizer consisting of a linear polarizer and a quarter-waveplate (QWP) for 546 nm. Two orthogonal CPELs were measured by rotating the QWP by $\pm 45^\circ$ with respect to the linear polarizer. All measurements were carried out in ambient environments after encapsulation.

Results and discussion

LPPL characteristics

Prior to the investigation of the CPEL, the aligning property of the F8BT on the rubbed AL22636 was confirmed by the OLED without a chiral dopant *via* a dissymmetry of the LPPL and phase retardation. The aligned F8BT emits linearly polarized light along the rubbing direction and the intensity ratio of the parallel component to the perpendicular one of the emitted light implies a degree of linear polarization. From the LPPL spectra in Fig. 2a, the degree of the linear polarization was evaluated to be 0.88 at 546 nm. In addition, a birefringence of the aligned F8BT was determined by the phase retardation of the mesogenic F8BT using the PEM method, where the intensity ratio of the first and second harmonics of the transmitted intensity passing through the sample and the PEM under crossed polarizers determined the phase retardation (see the ESI†).¹⁹ The phase retardation B as a function of the rotation angle θ with respect to one of the crossed polarizers is measured as shown in Fig. 2b and fitted by the following equation:²⁰

$$B(\theta) = \tan^{-1} \left[\frac{2 \sin B_0 \cos 2\theta}{1 - \cos 4\theta + \cos B_0 (1 + \cos 4\theta)} \right]$$

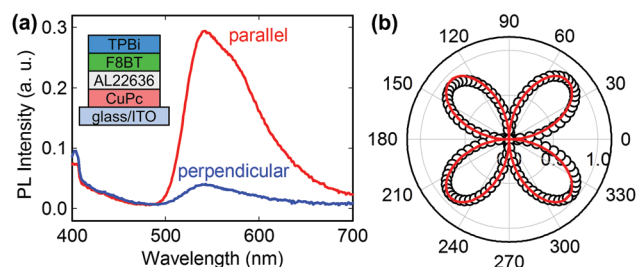


Fig. 2 (a) LPPL spectra for the OLED sample without the S5011. (b) The measured phase retardation (symbols) and the least-square-fit (solid line) as a function of the rotation angle.

Here, $B_0 (= 2\pi\Delta nd/\lambda)$ is an effective phase retardation of a thin film with thickness d and birefringence Δn at wavelength λ . It should be noted that the phase retardation, induced by the alignment layer and the TPBi layer, is negligible. The birefringence of the F8BT was 0.67 at 546 nm. The degree of the linear polarization and the birefringence are necessary to evaluate the dissymmetry g factor of the CPEL.

CPEL characteristics

EL spectra, textures, and the corresponding g factors of the OLEDs with different TPBi thicknesses are depicted in Fig. 3. At a wavelength of 546 nm, the difference between the intensities of LHCP and RHCP light first increases, reaches a maximum at a certain thickness (Fig. 3a and b), and then decreases (Fig. 3c) with increasing TPBi thickness, which is directly associated with the dissymmetry g factor as shown in Fig. 3d. It should be noted that the dissymmetry g factor at 546 nm was determined using a QWP at 546 nm and the spectrum intensity of the OLEDs at 546 nm. Here, the upper and lower images in each graph depict textures under LHCP and RHCP light, respectively.

In Fig. 3c, differing from Fig. 3a and b, a strong emission of both circular polarizations nearly around 400 nm was observed and, in addition, an inversion of the CP dissymmetry was observed between 420 nm and 520 nm. The strong emission of around 400 nm is attributed to an emission of the TPBi with a larger bandgap as shown in Fig. 1b, which means that the dominant emission (electron-hole recombination) zone of the OLED with a 50 nm TPBi layer is placed within the TPBi layer. As there was no observation of peak around 400 nm for the OLEDs with thinner TPBi than 20 nm (observation of the only F8BT emission), the clear inference is that the emission zone moves toward the TPBi (or the cathode) from the F8BT layer

upon increasing the thickness of the TPBi layer. Since the LUMO level of the TPBi is greater than that of the F8BT as shown in Fig. 1b, electron injection is much hindered and the electron-hole recombination zone will move toward the cathode at the thicker TPBi layer. It should be noted that the emitted light from the TPBi layer is randomly polarized due to no observation of any orientational ordering in the TPBi film. The randomly polarized TPBi emission exhibits the same intensities for both LHCP and RHCP light.

The inversion of the CP dissymmetry mainly originated from the absorption by the F8BT. The emission spectrum of the TPBi and the absorption spectrum of the F8BT were strongly overlapped in the range from 410 nm to 500 nm (see the ESI†). The randomly polarized light emitted from the TPBi is absorbed to the birefringent medium of the F8BT, and the orthogonal component of light is propagated to the twisted medium of the F8BT. As a result, the orthogonal CP light is enhanced in the range from 410 nm to 500 nm. The subtle difference in wavelengths between the inversion of the CP dissymmetry and the absorption of the F8BT would be related to the larger refractive index of F8BT at a shorter wavelength regime.

As shown in Fig. 3d, the dissymmetry g factor first increases, reaches a maximum at 20 nm thickness, and then decreases with increasing TPBi thickness. Based on our previous model,⁶ the dissymmetry g factor is increased when the emission (electron-hole recombination) zone moves toward the cathode (reflector) for these given device parameters (degree of polarization, birefringence, thickness, total twisted angle, wavelength, etc.). For TPBi layers thicker than 20 nm, reduction in the g factor is mainly due to the TPBi emission with random polarization.

Analysis of g factor

To investigate an effect of the emission zone and the randomly polarized TPBi emission on the g factor, we evaluated the g factors for different TPBi thicknesses under an optical setup as shown in Fig. 4a. For the elliptically polarized light generated from the OLEDs, the intensity I^G at $\lambda = 546$ nm (green) as a function of the rotation angle θ of a QWP with respect to the polarizer is expressed by the following equation (see the ESI†):

$$I^G(\theta) = \frac{I_{F,P}^G}{4} [\cos^2 \phi \{3 + \cos(4\theta)\} + 2 \sin^2 \phi \sin^2(2\theta) - \sin(2\phi) \{2 \sin \delta \sin(2\theta) - \cos \delta \sin(4\theta)\}] + I_N^G$$

Here, $I_{F,P}^G$ and I_N^G are the intensities for the polarized F8BT emission and the total non-polarized emissions of both F8BT and TPBi at $\lambda = 546$ nm, respectively. It should be noted that the intensity at $\lambda = 400$ nm is dominant but the intensity at $\lambda = 546$ nm is still relevant in TPBi emission spectrum (see the ESI†). Measured intensities at $\lambda = 546$ nm (open circles) and a fitted result (solid line) for the OLED without the TPBi layer are shown in Fig. 4b. Here, I_N^G consists of the non-polarized F8BT emission at $\lambda = 546$ nm ($I_{F,N}^G$) and the randomly polarized TPBi emission at $\lambda = 546$ nm (I_T^G). From the fitted parameters ($I_{F,P}^G$, I_N^G , ϕ , and δ) the dissymmetry factor g can be evaluated (see the ESI†). As shown in Fig. 4c, the evaluated g factors (open squares)

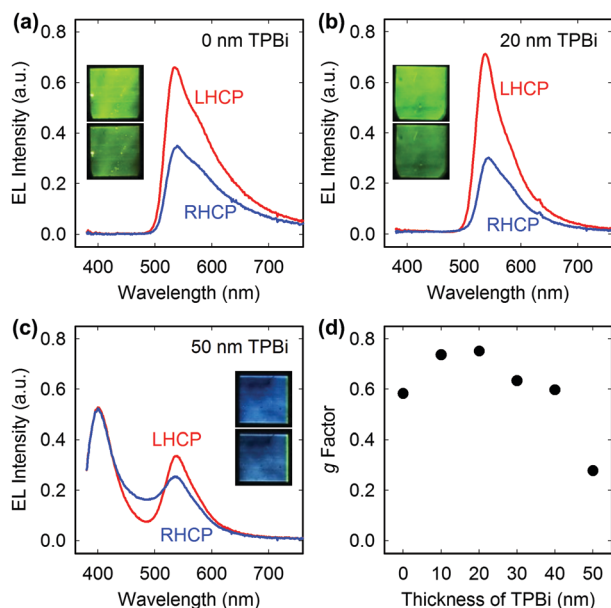


Fig. 3 (a–c) CPEL spectra for the OLED samples with various thicknesses of the TPBi under a circular polarizer. (d) The dissymmetry g factor at a wavelength of 546 nm as a function of thickness of the TPBi.

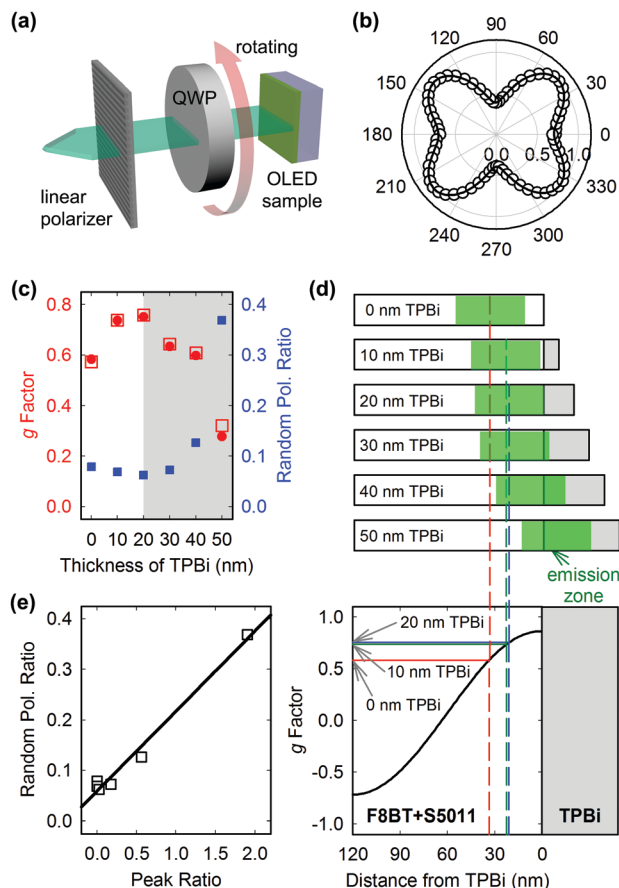


Fig. 4 (a) Experimental setup for evaluating the polarization state of emitted light from the OLEDs, and (b) the measured intensity (symbol) and the fitted result (solid line) of the OLED sample with zero-thickness TPBi as a function of the rotation angle of the QWP. (c) The directly measured g factor (filled circles) and the evaluated g factor (open squares) from (b), and a ratio of random polarization (filled squares) as a function of the thickness of the TPBi. (d) Schematic diagram of movement of the emission zone and the simulated g factor (solid curve) as a function of thickness of the TPBi. (e) The ratio of random polarization as a function of a ratio of the intensity at 400 nm to that at 546 nm.

are in good agreement with the measured g factors (filled circles). Also, a ratio (R_N) of the random polarization considering the randomly polarized TPBi emission at $\lambda = 546$ nm is defined by the following equation:

$$R_N = \frac{I_N^G}{I_{F,P}^G + I_N^G} = \frac{I_{F,N}^G + I_T^G}{I_{F,P}^G + I_{F,N}^G + I_T^G}$$

R_N was evaluated from the fitted parameters for $I^G(\theta)$ and is depicted in Fig. 4c (filled squares). The ratio of the random polarization is dramatically increased for TPBi layers thicker than 20 nm, where the g factor is decreased (shaded region). Such an increase in the R_N and decrease in the g factor are due to the TPBi emission with random polarization as shown in Fig. 3c. In addition, the increase in the TPBi emission implies that the emission zone moves toward the TPBi (or the cathode) from the F8BT layer by increasing the thickness of the TPBi layer.

For only F8BT emission, the g factor associated with the emission zone could be analytically calculated with the device parameters such as the degree of polarization of the emission, birefringence, thickness, and total twisted angle of the F8BT layer based on the Müller matrix analysis for the twisted birefringent medium (see the ESI†).⁶ Here, light emitted at a certain position within the EML propagated toward anode and cathode with the same probability while experiencing the twisted birefringent medium. The propagated light toward the cathode was reflected from the cathode and propagated again while experiencing the entire twisted birefringent medium in reverse. Finally, the g factor was calculated from the sum of Stokes parameters for both propagated lights (propagation lights to anode and cathode). The calculated g factor as a function of the distance of an emission zone from the TPBi layer and the schematic diagram of the emission zone for various thicknesses of the TPBi layer are depicted in Fig. 4d. The emission zone within the F8BT was estimated by comparing the calculated and measured g factors. For thicker TPBi cases involving the TPBi emission, the movement of the emission zone toward the TPBi layer was confirmed by increasing the peak intensity ($\lambda = 400$ nm), which was not observed in the thinner TPBi (pure F8BT emission). To confirm that the g factor reduction is attributed to the TPBi emission for thicker TPBi samples, we investigated the peak intensity (I_T^B) of the TPBi emission at $\lambda = 400$ nm (blue) as a function of the TPBi thickness. For normalization of the peak intensity for each sample, a ratio (R_{peak}) of the peak intensity at $\lambda = 400$ nm to that at $\lambda = 546$ nm is defined by the following equation:

$$R_{\text{peak}} = \frac{I_T^B}{I_{F,P}^G + I_{F,N}^G + I_T^G}$$

Assuming that $I_T^G = \alpha I_T^B$ (α is a constant), that is, the TPBi emission (I_T^G) at $\lambda = 546$ nm is linearly proportional to the TPBi emission (I_T^B) at $\lambda = 400$ nm, the random polarization ratio (R_N) is linearly proportional to the peak intensity ratio (R_{peak}) defined by the following equation:

$$R_N = \alpha R_{\text{peak}} + \beta$$

Here, β is a constant and means the random polarization ratio when no TPBi emission occurs. Such linearity is in good agreement with the experimental results as shown in Fig. 4e. The parameters of α and β were fitted to be 0.158 and 0.059, respectively. The fitted value β matched well with the results of $I_{F,P}^G$ and I_N^G for the thinner TPBi samples (see the ESI†). The fitted value $\alpha = I_T^G/I_T^B$ is slightly higher than the ratio of peak intensity at the pure TPBi emission spectrum (see the ESI†) due to spectrum broadening by stacking the TPBi on the F8BT with a smaller bandgap.

Conclusions

We investigated the relationship between the g factor and the position of the emission zone by controlling the thickness of the TPBi acting as the HBL and the EIH, and analysed the

Müller matrix analysis. For the polarized EML emission, the g factor increased when the emission zone moved toward the cathode upon increasing the TPBi thickness. However, the TPBi emission was observed and the g factor was reduced in thicker TPBi cases. The reduction in the g factor was due to the non-polarized TPBi emission and was quantitatively expressed with the ratio of non-polarized intensity to polarized one and the peak ratio of the emissions at the EML and the TPBi. This approach opens a new door to improve the g factor (enhance the OLED luminance in anti-reflection environments) for a given EML and to directly probe the emission zone with no additional layer and no performance degradation.

Conflicts of interest

There are no conflicts of interest to declare.

Acknowledgements

This work is supported by the KDRC (Korea Display Research Consortium) support program for the development of future device technologies for display industry.

Notes and references

- M. Jandke, P. Strohriegel, J. Gmeiner, W. Brütting and M. Schwoerer, *Adv. Mater.*, 1999, **11**, 1518–1521.
- U. Mitschke and P. Bäuerle, *J. Mater. Chem.*, 2000, **10**, 1471–1507.
- M. O'Neill and S. M. Kelly, *Adv. Mater.*, 2011, **23**, 566–584.
- D.-M. Lee, Y.-J. Lee, J.-H. Kim and C.-J. Yu, *Opt. Express*, 2017, **25**, 3737–3742.
- R. Singh, K. N. N. Unni, A. Solanki and Deepak, *Opt. Mater.*, 2012, **34**, 716–723.
- D.-M. Lee, J.-W. Song, Y.-J. Lee, C.-J. Yu and J.-H. Kim, *Adv. Mater.*, 2017, **29**, 1700907.
- C. Wagenknecht, C.-M. Li, A. Reingruber, X.-H. Bao, A. Goebel, Y.-A. Chen, Q. Zhang, K. Chen and J.-W. Pan, *Nat. Photonics*, 2010, **4**, 549–552.
- Y. Yang, R. C. da Costa, M. J. Fuchter and A. J. Campbell, *Nat. Photonics*, 2013, **7**, 634–638.
- F. Zinna, M. Pasini, F. Galeotti, C. Botta, L. D. Bari and U. Giovanella, *Adv. Funct. Mater.*, 2017, **27**, 1603719.
- C. Peng, A. Salehi, Y. Chen, M. Danz, G. Liaptsis and F. So, *ACS Appl. Mater. Interfaces*, 2017, **9**, 41421–41427.
- Y. Zhang, J. Lee and S. R. Forrest, *Nat. Commun.*, 2014, **5**, 5008.
- C. Coburn, J. Lee and S. R. Forrest, *Adv. Opt. Mater.*, 2016, **4**, 889–895.
- W. Song, W. Lee, K. K. Kim and J. Y. Lee, *Org. Electron.*, 2016, **37**, 252–256.
- U. S. Bhansali, H. Jia, M. A. Q. Lopez, B. E. Gnade, W.-H. Chen and M. A. Omary, *Appl. Phys. Lett.*, 2009, **94**, 203501.
- K. S. Yook and J. Y. Lee, *J. Ind. Eng. Chem.*, 2010, **16**, 181–184.
- M. C. Gather, M. Flämmich, N. Danz, D. Michaelis and K. Meerholz, *Appl. Phys. Lett.*, 2009, **94**, 263301.
- Y. Chen and S.-T. Wu, *J. Appl. Polym. Sci.*, 2014, **131**, 40556.
- S. I. Jo, Y. Kim, J.-H. Baek, C.-J. Yu and J.-H. Kim, *Jpn. J. Appl. Phys.*, 2014, **53**, 03CD04.
- Hinds Instruments, PEM-100 Technical Note.
- J.-H. Lee, C.-J. Yu and S.-D. Lee, *Mol. Cryst. Liq. Cryst.*, 1998, **321**, 317–322.